This article has been published in the Journal of Applied Physiology. The final publication is available at Pubmed via https://doi.org/10.1152/japplphysiol.00803.2019

Comprehensive Stereological assessment of the human lung using multi-resolution computed tomography

Dragoş M. Vasilescu[1], André B. Phillion[2], Daisuke Kinose[1], Stijn E. Verleden[3], Bart M. Vanaudenaerde[3], Geert M. Verleden[3], Dirk Van Raemdonck[3], Christopher S. Stevenson[4], Cameron J. Hague[5], MeiLan K. Han[6], Joel D. Cooper[7], Tillie-Louise Hackett[1*], James C. Hogg[1*]

[1]Centre for Heart Lung Innovation, The University of British Columbia, Vancouver, Canada;
[2]Materials Science and Engineering, McMaster University, Hamilton, Canada
[3]Leuven Lung Transplant Unit, KU Leuven and UZ Gasthuisberg, Leuven, Belgium;
[4]The Lung Cancer Initiative at Johnson and Johnson
[5]Department of Radiology, The University of British Columbia, Vancouver, Canada
[6]University of Michigan, Ann Arbor, MI, USA
[7]Department of Thoracic Surgery University of Pennsylvania, USA

Keywords: Human; Lung; Computed Tomography; microCT; Stereology

Author Contributions

Tissue collection and processing was performed by DMV, DK, SEV, MKH, DVR and JDC. Sample imaging was performed by DMV, ABP, MKH, and CJH. Image processing was performed by DMV and ABP. Image analysis and statistical analysis was performed by DMV, TLH and JCH. TLH and JCH have contributed equally to the study. Data interpretation and manuscript preparation was performed by all authors.

*Correspondence to: Dr. Dragoş Mihai Vasilescu, Centre for Heart Lung Innovation, University of British Columbia, St Paul's Hospital, Vancouver, BC V6Z 1Y6, Canada. **Dragos.Vasilescu@hli.ubc.ca**

Running Head: Stereological assessment of the human lung via CT

Descriptor: Human Lung

Word Count: 4243

Funding: DMV is supported by Canadian Thoracic Society and Alpha-1 Foundation fellowships.

TLH is supported by a Canadian Institutes for Health Research and Michael Smith Foundation for Health Research New Investigator awards. MKH is supported by a National Institutes of Health R01 HL122328 as well as a K24 HL138188. The study was in part funded through investigator initiated grants from Johnson & Johnson.

New & Noteworthy

For over 50 years, stereology has been used as the gold standard to quantify the three-dimensional anatomy of the human lung. Traditionally, stereology has been applied to lung casts, and two-dimensional light and electron microscopy images. However, such techniques are labor intensive involving fixation, embedding, and sectioning of samples, which has prevented extensive studies, especially when assessing changes with disease.

This study provides a method to apply stereology to multi-resolution, volumetric computed tomography (CT) images. The stereological-sampling cascade enables macroscopic measurements obtain using multi-detector computed tomography (MDCT, ~800μm resolution) on explanted air-inflated lung specimens, to be directly linked with high-resolution measurements obtained using microCT (<11μm resolution) on frozen lung samples. The method yielded a comprehensive quantitative dataset on the small airways and parenchymal lung structures within the healthy human lung, highlighting the differences between male and female lungs, which provides reference data for future pathological studies to assess lung disease.

Abstract

RATIONALE: The application of stereology to lung casts and 2-dimensional microscopy images is the gold standard for quantification of the human lung anatomy. However, these techniques are labor intensive involving fixation, embedding and histological sectioning of samples and thus, have prevented comprehensive studies.

OBJECTIVE: To demonstrate the application of stereology to volumetric multi-resolution computed tomography (CT) to efficiently and extensively quantify the human lung anatomy.

METHODS: Non-transplantable donor lungs from individuals with no evidence of respiratory disease (n=13), were air inflated, frozen at 10cmH_2O, and scanned using CT. Systematic uniform random (SUR) samples were taken, scanned using microCT, and assessed using stereology.

RESULTS: The application of stereology to volumetric CT imaging enabled comprehensive quantification of total lung volume, volume fractions of alveolar, alveolar duct, and tissue, mean linear intercept, alveolar surface area, alveolar surface area density, septal wall thickness, alveolar number, number-weighted mean alveolar volume, and the number and morphometry of terminal and transitional bronchioles. Using this dataset, we found that women and men have the same number of terminal bronchioles (last generation of conducting airways), but men have longer terminal bronchioles, a smaller wall area %, and larger lungs due to a greater number of alveoli per acinus.

CONCLUSIONS: The application of stereology to multi-resolution CT imaging enables comprehensive analysis of the human lung parenchyma that identifies differences between men and women. The reported dataset of normal donor lungs aged 25-77 years, provides reference data for future studies of chronic lung disease to determine exact changes in tissue pathology.

I. Introduction

To understand how disease alters the normal architecture of the human lung and how it can affect lung function, it is imperative to have robust reference data of normal lung anatomy. Several stereology-based studies have provided quantitative information about the anatomy of the human lung using 2-dimensional (2D) light, and electron microscopy, but these studies involved labor intensive fixation, embedding and histological sectioning techniques(5, 6, 57, 10, 11, 24, 33, 51–53, 56). In recent years, volumetric imaging techniques such as computed tomography (CT) now offer the possibility to obtain high-resolution 3D images of the entire thorax within a single breath hold(26). Volumetric CT imaging has the advantage that the spatial relationship of structures is maintained, enabling quantification of multiple parameters such as lung volume, regional gas volume, and bronchovascular morphometry to be obtained(13, 14, 58).

The current limitation of thoracic CT imaging is that the 800-1000μm resolution(23) does not allow visualization of the smallest lung structures such as the peripheral generations of conducting airways, the terminal bronchioles (mean diameter of 487μm(29)), alveolar ducts or alveolar septae (~12μm)(6). The application of microCT imaging with a resolution as high as 1μm, has permitted volumetric imaging of human lung tissue samples to visualize small airways, alveolar structures(25, 50), and quantify small airways disease(22, 29, 48).

To date, stereology has only been applied to microCT images to quantify the 3D architecture of the whole mouse lung(45, 46) and the small airways in ex-smokers with and without chronic obstructive pulmonary disease (COPD)(22). As highlighted by the American Thoracic Society/European Respiratory Society (ATS/ERS) guidelines(15) it is essential that controlled inflation, fixation and systematic uniform random (SUR) sampling are applied to ensure that samples are representative of the whole lung. To enable the assessment of disease it is essential

that a comprehensive dataset of stereological measures for the whole lung be available from a reference cohort lungs from individuals free of respiratory disease.

The present study describes a detailed methodology for SUR sampling of un-fixed, frozen human lungs, using multi-resolution volumetric CT imaging that rigorously adheres to the ATS/ERS guidelines for stereological sampling(15). Due to the application of volumetric multi-resolution CT imaging, this is the first study to analyze: volume fractions of alveoli, alveolar ducts, and tissue, mean linear intercept, alveolar surface area, alveolar surface area density, septal wall thickness, alveolar number, number weighted mean alveolar volume, as well as total number and morphometry of terminal and transitional bronchioles per lung, within the same lung which has never been achieved using existing methodologies. We demonstrate how a detailed stereological assessment of the lung parenchyma identifies anatomical differences in the lung structure of women and men, which has important implications for how alterations in lung structure are assessed in chronic lung diseases.

II. Methods

a. Lung Specimens

Donor lungs (n=13) without known respiratory diseases were collected through the University of Pennsylvania (n=7), University of Michigan (n=3), and Katholieke Universiteit Leuven (n=3). Lungs were released for research purposes if a transplant could not happen in time and informed consent was obtained from the donors in accordance with Belgian state legislation, where all suitable candidates automatically become donors, or from the donors next-of-kin in North America following a protocol outlined in the Gift of Life Donor Program (http://www.donors1.org). Lungs were archived in a registry approved by the Providence Health Care Research Ethics Board (H00-50110), University of British Columbia. The donor demographic data are listed in table 1.

Immediately after excision, a vascular graft tube is sewn to the main stem bronchus which is then connected to a tight underwater seal to inflate the lung. Lungs were inflated with air to a transpulmonary pressure of 30cmH_20 to ensure alveolar recruitment, then held at 10cmH_2O while rapidly frozen in liquid nitrogen vapor for 1 hour (Figure 1A). To obtain the total lung volume (V(lung)) lungs were imaged frozen using CT (120kV, 250mAmps, 1sec exposure time, slice thickness 0.625mm, average in plane pixel size of 0.7x0.7mm, Figure 1B). A radiologist (CJH) scored all specimen CT scans for airway abnormalities, emphysema, and interstitial abnormalities. Each lung was then cut into 2cm thick consecutive axial slices from apex to the base, on dry ice as indicated by the yellow lines in figure 1A using a pre-cooled commercial grade meat band saw. All slices were photographed at the same magnification with a reference scale which is crucial for subsequent sampling using the images, and stored at -80˚C.

b. Systematic Uniform Random (SUR) Sampling

Image registration was performed to match the orientation of the *ex-vivo* lung CT scan with the photographs of the cut lung slices (Figure 1C and D) using a custom program developed in Matlab (MATLAB Release 2016b, The MathWorks, Inc., USA). A SUR sampling method(15) was applied by superimposing a line grid (225mm^2) on the photographs of all lung slices (figure 1D). Connective tissue, large airways and blood vessels, that would represent more than 75% of a sample, were excluded from the sampling, yielding X potential sampling sites on all lung slices (on average 400 sites per lung, see example of all remaining intersection points of the line grid in figure 1D). Using a custom made hole punch device, 10 cylindrical tissue cores, 16mm in diameter and 20mm in height, were extracted across the lung volume (X / 10) using a random starting point which enabled a systematic uniform distribution. A total of 130 tissue cores were obtained across all lungs. The location of all SUR samples was translated to the CT scan (Figure 2A), to generate

a density histogram of the whole lung and each SUR sample (Figure 2B). Compared to *in-vivo* CT scans of the normal lung with a distribution peak at -850HU, the excised lungs lack blood flow and thus the peak is shifted to -910HU as previously reported(7, 32, 49).

c. MicroCT imaging

The frozen SUR samples were imaged with a microCT scanner (XT H 225ST, Nikon, USA) using a recently developed and validated cryo-microCT stage (Parameters: 40kV, 350µA, Molybdenum target, 500ms exposure time, and a gain of 32dB) resulting in an isotropic voxel size of 11µm(47).

d. Stereology

Reference Volumes

The total lung volume was calculated using semi-automatic image segmentation performed on the ex vivo lung CT scan, excluding the main stem bronchus and surrounding connective tissue (see 3D rendering of the lung segmentation in figure 1B). The total parenchymal volume was calculated by selecting 10 systematic uniform randomly (SUR) selected slices from the apex to the base of the *ex vivo* lung CT scan. A point grid of 100mm^2 was superimposed onto each of the 10 slices (see figure 1C) and the total number of points falling on parenchyma and non-parenchyma were counted. The ratio of points falling on parenchyma versus total number of points on lung (parenchyma + non-parenchyma) was used to determine the parenchymal volume fraction (Vv(par/lung)). The parenchymal volume fraction was then multiplied with the total lung volume to calculate the volume of parenchymal tissue used as reference volume to calculate alveolar surface area and total number of alveoli as previously described(15, 46).

Stereological Counts

To conduct stereological assessment on each lung tissue core, 10 SUR cross-sectional images were extracted from each microCT scan. Using a custom software for stereological counting on

microCT (Computer Assisted Stereology, developed by our lab in Matlab), a line grid (1mm long lines in a checkered pattern) was overlaid on each image to determine the number of intercepts within each line(5, 46, 51, 52) (Figure 3A). To obtain volume fractions of the parenchymal components each end point of each line was assigned as either alveolar, alveolar duct, tissue or non-parenchymal tissue (vessels and airways) which was excluded, as demonstrated in Figure 3A. From the number of lines and intercepts it is possible to calculate the mean linear intercept (Lm) and the alveolar surface area density (Sv(alv/lung)) as previously described(20, 21, 30, 31, 46). To calculate alveolar surface area, the alveolar surface area density is multiplied with the tissue volume per sample (volume fraction of tissue x sample volume) (15, 30, 46). To calculate the average septal wall thickness, the volume fraction of alveolar tissue volume is multiplied by 2 and divided by the alveolar surface density(46, 51).

Estimation of alveolar number was achieved by application of the physical disector approach(17, 33) to the microCT scans as previously described(45) using the STEPanizer program(43). The number of alveoli were estimated using 20 pairs of SUR cross-sectional images which were subsampled for generating a set of 160 (1.65mm x 1.65mm) disectors with a height of 22µm(43). Approximately 160 subsampled disectors were needed to obtain a total count of roughly 200 events per tissue sample, which has been shown to be sufficiently precise (8, 16). The paired SUR images were loaded into the STEPanizer program(43) and a counting frame was projected on each image. As shown in Figure 3B (image A and image B), the number of appearing and disappearing alveolar wall bridges was then counted within the counting frames. The number of alveoli and number weighted mean alveolar volume were then calculated as previously described(29, 33, 45).

The volumetric 3D microCT scans were used to scroll through the airways present to first identify the transitional bronchioles (TrB), the first generation of respiratory bronchioles, which can be identified by containing alveolar openings in the airway wall(9), as shown in Figure 3C. Identification of the transitional bronchioles is an unambiguous method to strictly identify the transition from the respiratory zone to the last generation of conducting airways, termed the terminal bronchioles, as previously defined by Rodriguez et al.(38). Identification of transitional bronchioles subsequently enabled the parent airway to be counted as a terminal bronchiole (TB). The volume of the tissue samples was measured using a complete 3D segmentation of the microCT scan. The numbers of terminal and transitional bronchioles per milliliter of lung (TB/ml and TrB/ml, respectively) were calculated by dividing the number of respective bronchioles by the sample volume. When TB/ml and TrB/ml were multiplied with the total lung volume obtained from the CT scan, the total number of bronchioles per lung was calculated. As previously described by Tanabe et al.(41), images perpendicular to the skeleton line of terminal bronchioles are extracted. To enable comparison between all airways we select images at 10% increments along the branch length. The initial start point is at 50% of the branch, followed by 10% increments towards the two end points, i.e. 40% and 60%, 30% and 70%, 20% and 80%, ending with 10% and 90%, resulting in 11 images along the branch length. The extracted images are generally limited to a 4mm x 4mm field of view around the airway to enable the identification of neighboring structures. By extracting images at these consistent intervals, it is possible to assess airways at the same points along their branch length. Semi-automatic segmentation of the inner and outer airway wall enabled calculation of cross-sectional lumen area, wall thickness, wall area percent, circularity, and perimeter. The number of alveolar attachments was counted manually on all cross-sections and divided by the outer airway perimeter length to for normalization.

e. Statistics

The results are expressed as mean ± standard deviation (SD) values per sample or whole lung. T-tests were used to compare morphometric measures by sex, linear regression with a 95% confidence interval and Spearman rank test were used for all other tests; a p-value <0.05 was considered significant.

III. Results

a. Patient characteristics

The 13 donor lungs consisted of 3 left and 10 right lungs with an average lung volume of 2,883±721ml, obtained from 6 females and 7 males, with an average age of 57±16 years (range 25 to 77 years). All donors died of non-respiratory causes, eight had no smoking history and five were ex-smokers with an average of 19±15 pack years. For all donors the average body height was 172±6cm, and average body weight was 94±22kg. No lung function measurements were available for any donor. All demographics data are presented in Table 1. Based on the radiological evaluation, three of the specimen showed upper-lung dominant mild emphysema (Cases 6, 10 and 12, table 1).

b. Comprehensive stereological assessment of the normal donor lungs

Table 2 compares the morphometric measurements obtained using our CT-stereology approach, to prior studies conducted using stereology on formalin-fixed tissue samples using histology and electron microscopy, whole lung casts, or representative sampling using microCT, on lungs inflated to similar pressure. All data from this study are also presented per case in table 3.

<u>Reference volume</u>

In this study, the average total lung volume was 2,883±721ml, which is comparable to previous studies of donor lungs with an average for all studies of 2,798±1,007ml. The volume fraction of

parenchyma (V_v(par/lung), excluding large airways and vessels visible on CT) measured on the CT images was 87±3%, which is comparable to the values reported in previous studies using images of gross lung specimens 90%(6) and 88%(56).

Terminal and Transitional Bronchioles

There was on average 7,697±2,910 terminal bronchioles per lung and 14,956±6,664 transitional bronchioles per lung. Haefeli-Bleuer et al., previously estimated a total number of 15,000 transitional bronchioles per lung, based on the average acinar volume measured on two lung casts of the left upper lobe(9). Using representative sampling and microCT imaging, McDonough et al. reported 22,300 terminal bronchioles per lung (4 donor lungs)(29) and Verleden et al., reported 17,427 terminal bronchioles per lung (7 donor lungs)(48), but no transitional bronchioles were counted in these two studies.

A total of 122 terminal bronchioles (n=68 in males and n=54 in females) from a subset of three randomly selected samples per case, were assessed in detail. The average terminal bronchiole branch length was 2.25±0.91mm, with an average lumen area of 0.28±0.19mm^2, and a maximum and minimum lumen diameter of 0.65±0.2mm and 0.52±0.17mm, respectively. The average terminal bronchiole had a wall area percent of 37.1±9.04%, a wall thickness of 0.06±0.02mm, and 11.48±2.65 alveolar attachments. These values are comparable to a prior study by Tanabe et al, who analyzed 38 TB's from random samples scanned using microCT from 7 donor lungs(40).

Airspace Measurements

The average Lm per lung was 348µm, as compared to 216µm by Thurlbeck who used formalin-fixed samples(42). Using microCT, McDonough et al.(29) and Verleden et al.(48), reported Lm's of 336µm and 269µm, respectively. In this study, the total alveolar surface area (S(alv,lung)) was 67±20m^2 per lung, which is in line with the study by Weibel(51) using light microscopy who

estimated an alveolar surface area of 63m^2 per lung, and the study by Gehr et al. using transmission electron microscopy (TEM) who reported an alveolar surface area of 72m^2 per lung(6). In contrast, Wiebe(56) and Thurlbeck(42) using light microscopy and formalin-fixed samples reported a total alveolar surface area of 31m^2 and 32m^2 per lung, respectively, at a comparable level of magnification to the current study.

The average alveolar septal wall thickness for the normal lung was 12±3μm. Gehr et al. previously used TEM to determine an air-blood barrier thickness of 2.2μm(6). As the alveolar septa generally consist of two air-blood interfaces, and a capillary lumen approximately the size of an erythrocyte (average diameter 7.2μm(44)), using the data provided by Gehr et al., the whole septal wall thickness would be approximately 12μm. The only other study to estimate septal wall thickness used the inverse of the alveolar surface density(2), which has been shown to incorrectly calculate septal wall thickness(6, 15, 46). However, using the data of Coxson et al., for alveolar surface density and tissue volume fraction for smokers with normal lung function, we calculated an average septal wall thickness of 13μm by applying the same formula used in the current study.

Parenchymal Components

The volume fraction of the parenchymal components in the normal lung consisted of 71% alveoli, 13% alveolar duct space, and 16% alveolar tissue. The only previous studies to estimate the volume of fraction of alveoli were Gehr et al. who reported an alveolar volume fraction of 78%(6) and Ochs et al. who reported 70%(33).

We determined the total number of alveoli within the normal lung to be 106±41 million per lung, whereas Weibel reported 294 million per lung(51) and Ochs 240 million per lung(33) using light microscopy. Using representative sampling and microCT images with 16μm resolution, McDonough has estimated a total of 80 million alveoli per lung(28). Further, the number weighted

mean volume of an alveolus was $18x10^6 \mu m^3$ compared to Ochs et al. who reported $4x10^6 \mu m^3$ using light microscopy(33).

c. Comparison of Lung Measures by Sex

There was no difference between males and females for the total number of terminal (Figure 5A) or transitional bronchioles (Figure 5B) per lung. However, terminal bronchioles in males had a longer branch length (Figure 5C, females: 2.02±0.67mm, males: 2.43±1.03mm), and a reduced luminal circularity (Figure 5D, females: 0.94±0.07, males: 0.94±0.03), whereas, terminal bronchioles in females had a significantly greater wall area percent (Figure 5E, females: 40.6±9.9, males: 34.4±7.2). There was no difference in the cross-sectional area (females: $0.31\pm0.25 mm^2$) or number of alveolar attachments per terminal bronchiole adjusted for perimeter (females: 12±3, males: 11±2), between males and females (Figure 5F and G).

While the mean volume of an alveolus (Figure 6A) was not different between males and females, the total alveolar surface area (Figure 6B) and number of alveoli were significantly greater in males compared to females (Figure 6C). When normalized by volume, these alveolar dimensions did not differ between males and females (Figures 6D and E), which indicates that men have a larger alveolar surface area and total number of alveoli, due to a larger total lung volume as shown in figure 6F.

d. Correlations of lung measures with lung volume, lung height, subject age and smoking history

There was a significant correlation of lung volume with alveolar surface area (Figure 7A) and number of alveoli (Figure 7B), but not with any other morphometric measures. Due to the SUR sampling design, and the extensive counting employed within each sample, it was possible to assess differences in morphometry over lung height, however no morphometric measures

correlated with lung height. Further, none of the lung measures correlated with age. In addition, there were no differences in any of the morphometric measures with smoking history except that the ex-smokers in this study had a greater number of terminal bronchioles per ml of lung ($p<0.05$, Figure 8).

IV. Discussion

To our knowledge the method described in this study is the first to enable the application of stereology to multi-resolution CT imaging, to obtain robust, high-precision quantitative data on the human lung. Further, the application of cryo-CT imaging of the human lung and tissue samples enabled the quantification of lung structures to occur without the requirement of tissue fixation. The resulting comprehensive quantitative dataset of lung anatomy from the lungs of a cohort of normal subjects aged 25-77 years, demonstrated several anatomical features of the lung parenchyma that were difference between men and women. Such analysis will be important in future studies of chronic diseases to determine the exact pathological changes that occur with chronic respiratory disease.

Prior to the recent application of volumetric microCT imaging of fixed, and dried lung samples(22, 25, 29, 46, 48) airway casts or extensive serial histological sectioning were used to study the 3D morphometry of the transitional bronchioles and acinar structures(9, 37). To count terminal and transitional bronchioles using stereology and volumetric imaging in this method, we applied the strict criteria suggested by Rodriguez et al.(38), and subsequently Haefli-Bleuer et al.(9), who defined transitional bronchioles as the first bronchiole along the airway tree in which the first alveolus occurs. One advantage of volumetric microCT imaging is that it allows the observer to easily identify individual alveoli or small groups of alveoli on the airway walls while browsing through the serial images, rather than extensive histological sections. Furthermore, 3D

datasets enable tracking of the branching airways so that the relationship of parent and daughter airways can be recorded as long as they remain in the field of view. Thus, as we have described previously(22), it is possible to identify the last generation of conducting airways, the terminal bronchioles, by assessing if one of the daughter airways is a transitional bronchiole containing alveoli in its wall. With this method it is possible to reproducibly count terminal and transitional bronchioles within the human lung using volumetric imaging. Using this definition we determined that on average there are 14,956 transitional bronchioles within the normal human lung. To our knowledge, the only other study to estimate the number of transitional bronchioles in donor lungs, was a study of lung casts by Haefli-Bleuer et al. in which they estimated the number of acini, using their definition(9). Using this approach the authors estimated there are 15,000 transitional bronchioles in the human lung which is almost exactly the same as our finding using microCT.

In terms of terminal bronchioles we counted on average 7,697 in the human lung. Based on a dichotomous airway branching, one would expect to find exactly half the number of parent terminal bronchioles to daughter transitional bronchioles. However, as shown by the diagram in Figure 3C a terminal bronchiole can bifurcate into a respiratory bronchiole and one conducting bronchiole in addition to the normal occurrence of two daughter respiratory bronchioles. Two previous studies using microCT have reported 22,300(29) and 17,427(48) terminal bronchioles within normal donor lungs. The main differences between these prior studies and the current study is that they did not use SURs sampling, account for tissue shrinkage, or use the unambiguous definition of Rodriguez et al.(38) for identifying transitional bronchioles to identify terminal bronchioles.

In terms of parenchymal structures, mean airspace size (Lm) is one of the most commonly used measurements to quantify airspace enlargement. A limitation of the measurement of Lm is that it

is not able to distinguish between alveolar air space and alveolar ducts(20), and can be significantly affected by inflation status, or elastic properties of the lung, the latter of which would also affect tissue shrinkage with fixation. However, in conjunction with the measure of parenchymal volume fraction and the total lung volume one can calculate the total alveolar surface area (tissue available for gas exchange)(15, 31, 33) and septal wall thickness(6), which are corrected for tissue volume in every sample, and therefore are not affected by inflation or elastic properties of the lung. Using volumetric imaging of frozen lung samples the measurements of alveolar surface area ($67m^2$) reported in this study is comparable to previously reported values ($63m^2$ and $72m^2$) obtained using light microscopy images on fixed tissue samples(6, 51). The 11µm image resolution provided by microCT was sufficient to estimate septal wall thickness (12µm), that was comparable to previous studies (Gehr et al. = 12µm, Coxson et al. = 13µm) performed at much higher resolutions than the current study(2, 6).

By measuring the volume fractions of alveoli and alveolar ducts it is possible to understand their influence on Lm measurements. As previously shown, with adequate magnification and resolution, it is possible to perform a relatively unbiased distinction between alveolar space and alveolar duct space(31). For example, to determine what contributes to an airspace enlargement (Lm) it is crucial to distinguish between changes in alveolar surface area or alveolar ducts, as the prior has a significant effect on the functional capacity of the lung. Further, differences in the percentage of alveoli, ducts, and parenchymal tissue have been shown to change with aging (51). The analysis of volume fractions of tissue will be important in future assessments of chronic lung diseases to understand the microscopic tissue pathology of early disease, in addition to the alterations in lung anatomy due to aging and sex. As volume fractions are not as sensitive to

resolution, our measurement of 71% alveolar volume fraction is comparable to 78% reported by Gehr et al. in which they used the much higher resolution provided by TEM(6).

In the current study we report 106±41 million alveoli per lung, whereas Weibel reported 294 million per lung(51) and Ochs 240 million per lung(33) using light microscopy. Using representative sampling and microCT images with 16μm resolution, McDonough et al estimated a total of 80 million alveoli per lung(28). Further, we report an average alveolar size of 18 $10^6 \mu m^3$ compared to 4 $10^6 \mu m^3$ by Ochs et al.(33). Several factors may explain the smaller number and larger size of alveoli, reported in this study. Firstly, using microCT the voxel resolution in this study was 11μm compared to the higher resolution in histological studies which may allow smaller alveoli to be counted. Additionally, the disector height in the current study was 22μm, while Ochs et al.(33) used a spacing of 9μm with histology. It is therefore possible that alveolar openings may have been missed. Further, the mean age of subjects in this study was 57 years and a reduction in the number of alveoli with age has previously been shown. Future studies with a larger age range of subjects will be required to answer this question.

When the anatomical structures of the lung were compared by sex, the data demonstrate that men and women have the same number of terminal bronchioles. Thus, as the lung has a predominantly bifurcating airway tree, males and females must have a similar total number of conducting airways to be able to have the same number of terminal bronchioles (last generation of conducting airways), despite men having larger lungs. The data also demonstrate that the number of alveoli is greater in men compared to women, but the average alveolar size is the same. Since the respiratory zone of the lung is divided into acini which start with the first generation of respiratory airways, termed the transitional bronchioles, and we report that the number of transitional bronchioles are the same in men and women, we conclude from the data that the acini

within men must therefore have a larger acinar volume to accommodate the greater number of alveoli present within the male lung (estimated by dividing the volume of parenchyma by the total number of transitional bronchioles; average: 200mm^3, men: 232mm^3 and female: 162mm^3). A greater number of alveoli in men also explains previous findings that have demonstrated that men have a higher diffusion capacity compared to women(34). Regarding the morphometry of the terminal bronchioles, males had a longer branch length compared to females, most likely to accommodate the larger acinar volumes and to enable the terminal bronchiole to reach the lobular center. Despite Dominelli et al. reporting that females have ~30% smaller cross-sectional area in the central airways than men(4), the cross-sectional area of the terminal bronchioles measured in this study was found to be similar in males and females.

The importance of airway wall thickness and its significant correlation with sex has been investigated by many studies with controversial results(1, 3, 27, 35, 49), but only a few studies have specifically looked into differences of airway wall measurements between males and females of healthy individuals to better understand baseline measures. Zach et al. reported that for the large conducting airways visible by thoracic CT, the wall area percent is influenced by sex(59), whereas Camp et al.(1), concluded that CT might not have the resolution necessary to detect such a subtle remodeling. By analyzing anatomically matched airways, Kim et al. have shown that the subsubsegmental airways of females have an higher WA% than males(19), and based on our microCT data, we confirm this difference is also present in the terminal bronchioles. The exact structural tissue component that results in thicker airway walls in females is still to be determined, and will require future histological study.

There are however some limitations to be noted in the study. The resolution of microCT provides many advantages for the detailed assessment of the lung anatomy, but such scans cannot

be performed *in-vivo* and are limited to resected lung specimens, preventing longitudinal assessment of the lung anatomy. The current study used donor lungs with no known respiratory diseases, however no lung function data were available for the donors preventing any correlations with the presented measurements. Three of the thirteen cases showed signs of mild radiologically defined centrilobular emphysema on the specimen CT scans. Several large cohort studies using clinical CT have reported that life-time never smokers, in addition to ex-smokers with preserved lung function, have evidence of mild emphysema(12, 39). Therefore, as the three donor lungs were representative of the emphysema observed within the normal population, and as the microCT assessment showed no significant differences from the normal range of non-smokers, they remained included in the study. Lastly, the 16mm x 20mm samples used in this study, resulted in a resolution of 11µm, thus, due to the partial volume effect, objects smaller than 11µm would be overestimated(15, 45, 51) (known as the coast of Britain effect(55)). However, the partial volume effect caused by the x-ray absorption occurring sub pixel sized objects especially at edges has some advantages. For example, partial-volume effects have been used to measure cracks in crystalline rocks(18) or pores in soil samples(36) that were considerably smaller than the pixel dimensions of the microCT images(54). Further, we have previously demonstrated that when measurements of septal wall thickness on histology are corrected for shrinkage due to tissue fixation and embedding, you obtain the same value as on a matched frozen microCT samples(47). To resolve the septal walls in greater detail, smaller tissue samples or interior microCT scans could be conducted to increase resolution.

In conclusion, volumetric multi-resolution CT imaging of the frozen lung combined with stereological sampling enables a comprehensive understanding of the complex human lung structure. This study reports several anatomical features of the lung parenchyma that are different

between men and women, which could not be identified using Lm alone. Such detailed stereological measurements of the alveoli, ducts and parenchyma will be crucial in future studies of chronic lung diseases to try to determine the exact changes in tissue pathology, especially early, microscopic disease lesions that cannot be detected by clinical CT.

V. Acknowledgements

The authors would like to acknowledge Dr. Arron Barlow from the Cellular Imaging and Biophysics Core for his help with microCT image acquisition, Dr. W. Mark Elliott and Darren Sutherland from the James Hogg Lung Registry, and Ms. Madeleine Downey for her dedication in helping to perform the stereological counting, all from the Centre for Heart Lung Innovation. The authors would also like to extend special thanks to Dr. Peter Paré for his invaluable comments and revisions. In addition, the authors would like to thank Mr. Derrick Horne from the UBC bio imaging facilities for his expertise on preparing tissue samples for imaging. We would like to thank Dr. Ewald R. Weibel for his mentorship and who was consulted numerous times on how to best translate the methodologies developed by himself and others for an accurate stereological assessment of the whole human lung using CT. His excellent guidance and feedback will be missed (From the Living History of Physiology compendium (https://www.the-aps.org/community/aps-membership/Living-History-of-Physiology?SSO=Y) here is an interview with Dr. Weibel (https://youtu.be/dBsNrUlE4GU)).

VI. Tables

Table 1.

Case	Lung Used [left / right]	Age [years]	Sex	Ethnicity	Body Height [cm]	Weight [kg]	Cause Of Death	Smoking History [pack years]	Specimen Volume [mL]
1	L	25	Female	Caucasian	165	107	Cardio-vascular arrest	7	1,740
2	R	29	Female	Black	NA	149	Cardio-vascular arrest	0	2,063
3	L	42	Male	Caucasian	178	75	Stroke	15	3,401
4	L	53	Male	Caucasian	165	65	Stroke	0	3,701
5	R	56	Male	Black	180	103	Cardio-vascular arrest	0	2,313
6	R	57	Female	Caucasian	170	65	Subarachnoid haemorrhage	NA	2,644
7	R	61	Male	Caucasian	178	102	Stroke	0	3,611
8	R	64	Male	Caucasian	178	98	Stroke	15	4,080
9	R	64	Male	Caucasian	175	81	Gunshot wound	NA	3,281
10	R	65	Female	Caucasian	175	100	Stroke	15	3,131
11	R	71	Female	Caucasian	168	95	Stroke	0	2,346
12	R	77	Female	Caucasian	163	91	Head Trauma	45	2,204
13	R	77	Male	Caucasian	175	90	Subarachnoid haemorrhage	0	2,968
Summary	**3L / 10R**	**57 ± 16**	**6F / 7M**		**172 ± 6**	**94 ± 22**			**2883 ± 721**

Table 2.

Measurements (per lung)	Present Study	Weibel 1963	Thurlbeck et al., 1967	Horsfield & Cumming 1968	Gehr et al., 1978	Haefeli-Bleuer et al., 1988	Wiebe et al., 1998	Ochs et al., 2004	McDonough et al., 2011*	Verleden et al., 2014	McDonough et al., 2015*
# Subjects	13	5	25	1	8	2	10	6	4	7	4
Study type	MicroCT	Histology	Histology	Airway Cast	Histology TEM	Airway Cast	Histology	Histology	MicroCT	MicroCT	MicroCT
Specimen inflation	Air	Formalin steam	Formalin	Cast material	GA	Cast material	Formalin	Formalin	Air	Air	Air
Sample preparation	Frozen	FFPE	FFPE	NA	JB-4	NA	FFPE	FFPE	GA fixed and dried	GA fixed and dried	GA fixed and dried
Age	57 ± 16	36 ± 26	53 ± 18	25	30 ± 9	Adults	71 ± 9	29 ± 9	54 ± 4	54 ± 12	54 ± 4
Smoking history	6 non-smokers 5 ex-smokers 2 NA	NA	NA	NA	NA	NA	NA	NA	2 non-smokers 2 ex-smokers	NA	2 non-smokers 2 ex-smokers

Lung volume [ml]	2,883 ± 721	2,510 ± 1,070	2,467 ± 716	--	2,170 ± 402	2,500 - 3,000[¥]	2,100 ± 400	1,534 ± 521	3,251 ± 261	3,300 ± 700	3,251 ± 261
V_v(par/lung) [%]	87 ± 3	91 ± 1	--	--	90 ± 0	--	88 ± 0	92 ± 3		--	0.89 ± 0.05
Terminal bronchiole number	7,697 ± 2,910	--	--	~13,996	--	--	--	--	22,300 ± 3,900	17,427 ± 6,577	--
Transitional bronchiole number	14,956 ± 6,664	--	--	--	--	13,000 – 16,000[¥]	--	--	--	--	--
Lm [µm]	348 ± 45	--	216 ± 28	--	--	--	--	--	336.81 ± 60.48	269 ± 28.00	--
S_v(alv/lung) [1/cm]	266 ± 41	--	--	--	371 ± 29	--	--	--	--	--	--
S(alv, lung) [m^2]	67 ± 20	63 ± 16	32 ± 8	--	72 ± 17	--	31 ± 6	--	--	--	--

τ(alvsep) [µm]	12 ± 3	--	--	--	12 ± 1[†]	--	--	--	--	--
τ(alv,tissue) [µm]	--	--	--	--	2 ± 1[‡]	--	--	--	--	--
V_v(alv/par) [%]	71 ± 3	60 ± 4	--	--	78 ± 3	--	--	70 ± 3	--	--
V_v(duct/par) [%]	13 ± 4	32 ± 5	--	--	--	--	--	--	--	--
V_v(tissue/par) [%]	16 ± 4	7 ± 1	--	--	--	--	--	--	--	--
N_v [1/mm^3]	42 ± 12	201 ± 99	--	--	--	--	--	170 ± 16	--	28 ± 4
N(alv) [10^6]	106 ± 41	294 ± 11	--	--	--	--	--	240 ± 89	--	80 ± 21
V(alv) [ml]	1,790 ± 531	--	--	--	3,386 ± 687	--	--	988 ± 328	--	--
$\overline{v}_N$(alv) [10^{6}µm^3]	18 ± 7	--	--	--	--	--	--	4 ± 0	--	--

NA – not applicable

GA = Glutaraldehyde

FFPE = formalin fixed and paraffin embedded

JB-4 = A water-soluble, glycol methacrylate based, plastic resin

“--" no data reported or measured in the study

TEM = transmission electron microscopy

¥estimated based on average lung volume and acinar volume.

†Calculated based on data provided in the study

‡value based on electron microscopy images

*****Both studies by McDonough et al. used the same cases, more measurements were performed for the later study.

Lm = mean linear intercept

S_v(alv/lung) = alveolar surface density

S(alv, lung) = total alveolar surface area

τ = wall thickness, alvsep = alveolar septa, alv,tissue = air-blood barrier, only visible with electron microscopes

V_v = volume fraction

N_v = alveolar density

$\bar{v}_N$(alv) = number weighted mean volume of an alveolus

Table 3.

Case	1	2	3	4	5	6	7	8	9	10	11	12	13	Average ± SD
Lung side	L	R	L	L	R	R	R	R	R	R	R	R	R	**3L / 10R**
Age [years]	25	29	42	53	56	57	61	64	64	65	71	77	77	**57 ± 16**
Pack years	7	0	15	0	0	0	0	15	0	15	0	45	0	**7 ± 13**
Lung volume [ml]	1,740	2,063	3,401	3,701	2,313	2,644	3,611	4,080	3,281	3,131	2,346	2,204	2,968	**2,883 ± 721**
V_v(par/lung) [%]	85	78	90	91	88	84	89	89	85	89	87	86	87	**87 ± 3**
TB per lung	8,453	4,649	13,203	6,709	3,833	8,036	9,428	8,907	3,191	10,372	4,948	8,275	10,057	**7,697 ± 2,910**
TrB per lung	17,129	8,439	27,363	13,634	7,534	16,223	17,466	18,355	5,637	21,847	8,246	10,251	22,308	**14,956 ± 6,664**
Lm [µm]	289	327	321	346	325	366	335	357	430	366	307	444	313	**348 ± 45**
S_v(alv/lung) [1/cm]	332	244	299	278	247	262	239	269	186	262	312	216	307	**266 ± 41**
S(alv,lung) [m^2]	49	39	91	94	50	58	77	98	52	73	64	41	79	**67 ± 20**
τ [µm]	12	20	13	12	12	12	10	12	15	13	8	11	10	**12 ± 3**
V_v(alv/par) [%]	69	67	70	71	70	69	79	70	68	72	71	67	76	**71 ± 3**
V_v(duct/par) [%]	11	8	11	13	15	15	10	13	18	11	16	21	9	**13 ± 4**
V_v(tissue/par) [%]	20	24	19	16	15	16	12	16	14	17	13	12	15	**16 ± 4**

N_v(alv/lung) [1/mm^3]	43	47	50	43	37	49	47	37	30	18	54	29	65	**42 ± 12**
N(alv,lung) [10^6]	63	76	155	145	75	108	150	136	84	51	111	56	168	**106 ± 41**
V(alv,lung) [ml]	1,019	1,086	2,143	2,386	1,426	1,539	2,533	2,559	1,905	1,996	1,457	1,267	1,955	**1,790 ± 531**
$\overline{\upsilon}_N$(alv) 10^6µm^3]	16	14	14	16	19	14	17	19	23	39	13	23	12	**18 ± 7**

TB = terminal bronchioles

TrB = transitional bronchioles

Lm = mean linear intercept

S_v(alv/lung) = alveolar surface density

S(alv, lung) = total alveolar surface area

τ = Septal wall thickness

V_v = volume fraction

N_v = alveolar density

$\overline{\upsilon}_N$(alv) = number weighted mean alveolar volume

VII. Figure Headings

Fig. 1

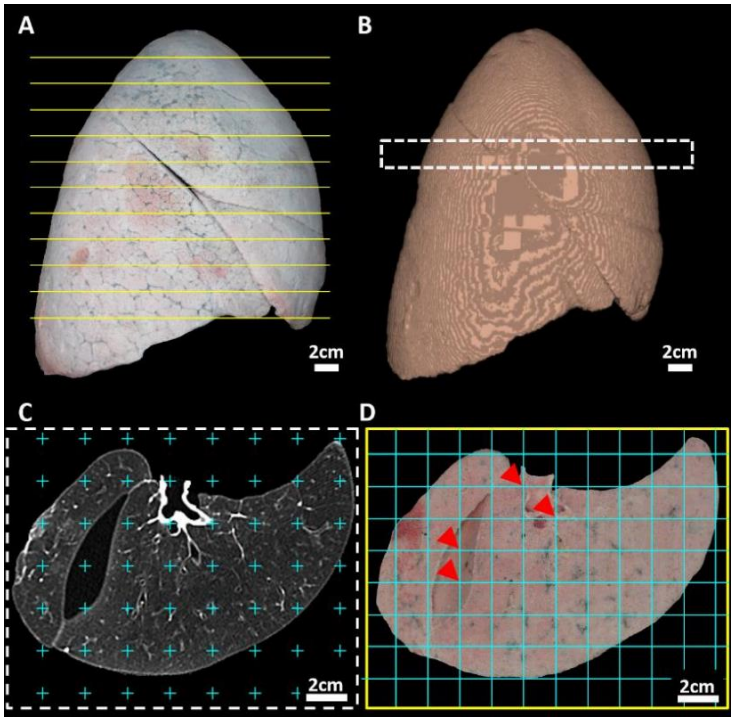

Fig. 2

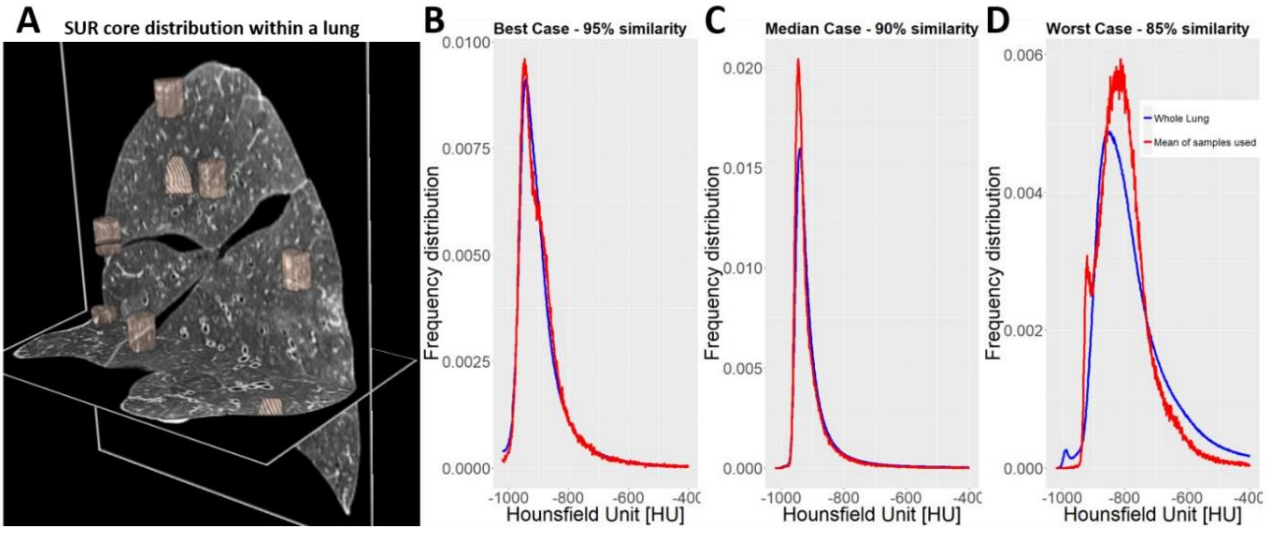

Fig. 3

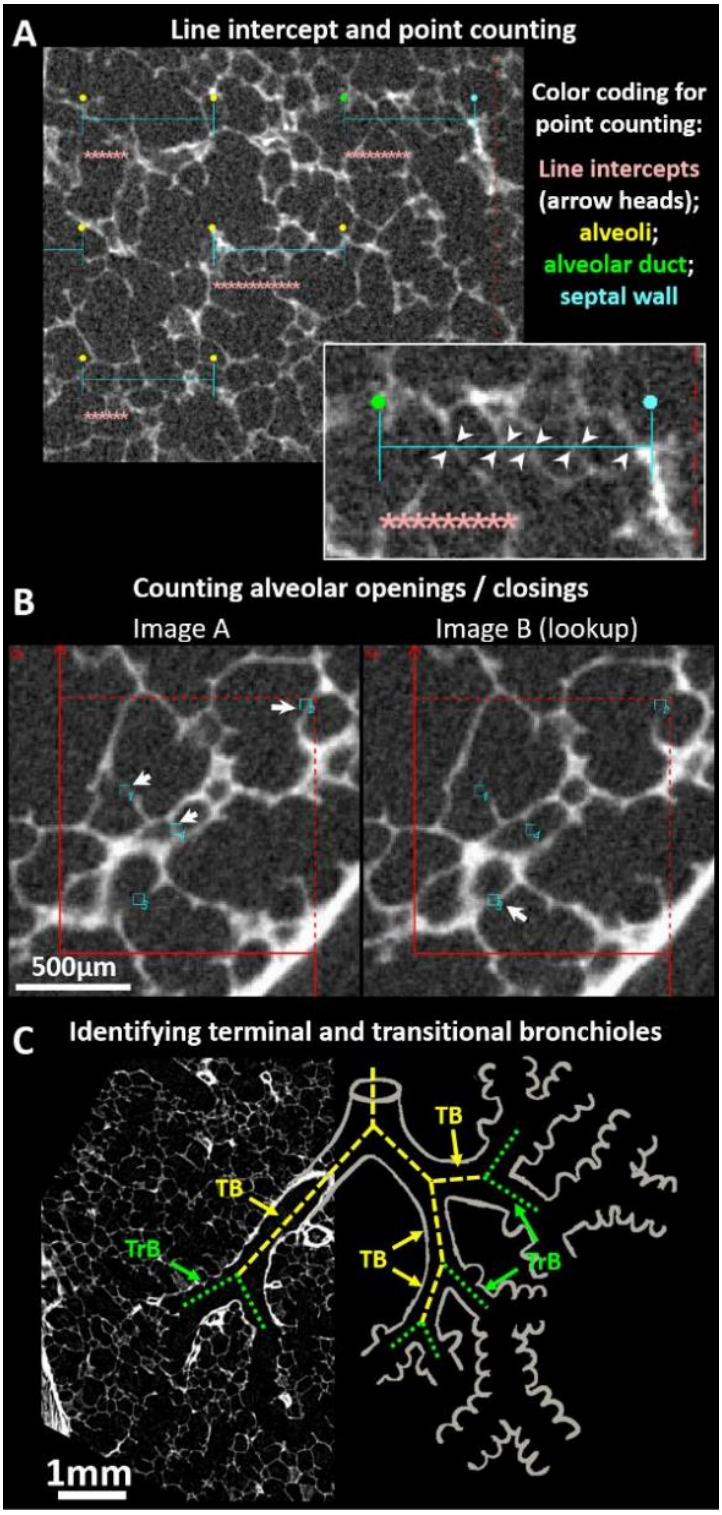
A
Line intercept and point counting
Color coding for point counting:
Line intercepts (arrow heads);
alveoli;
alveolar duct;
septal wall
B
Counting alveolar openings / closings
Image A
Image B (lookup)
500µm
C
Identifying terminal and transitional bronchioles
TB
TB
TB
TrB
TrB
1mm

Fig. 4

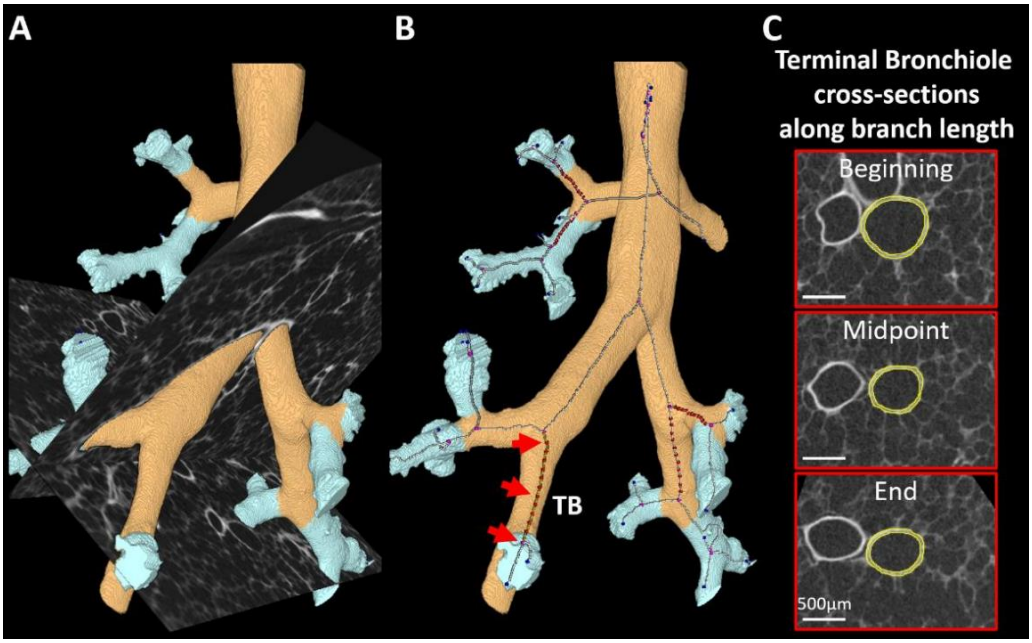
A
B
C
Terminal Bronchiole cross-sections along branch length
Beginning
Midpoint
End
TB
500µm

Fig. 5

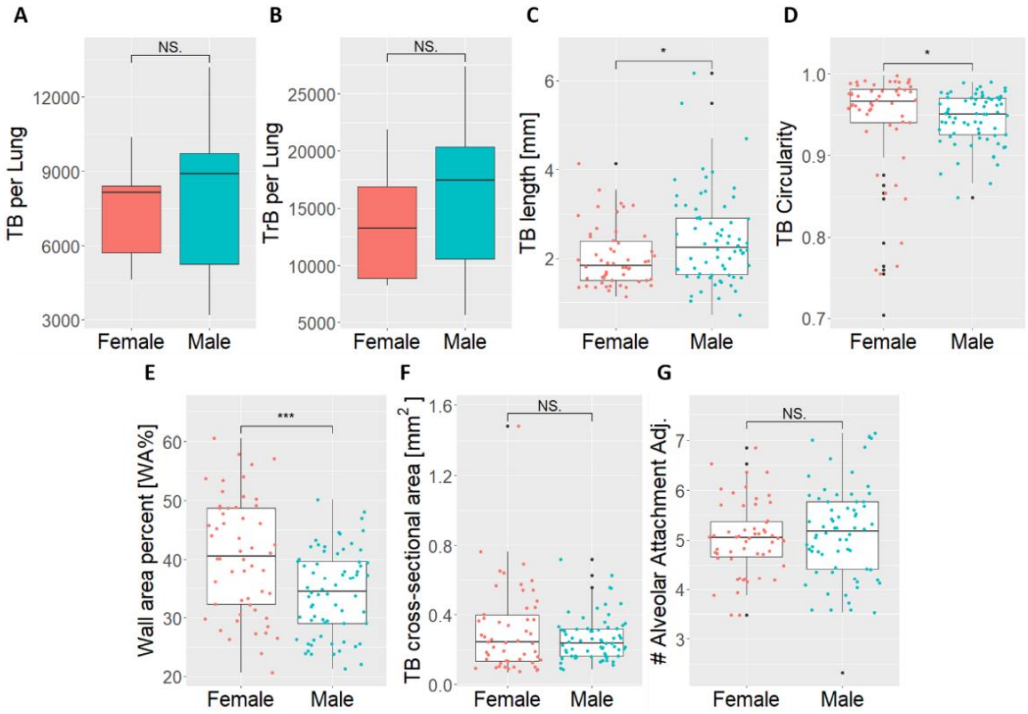
A
B
C
D
TB per Lung
TrB per Lung
TB length [mm]
TB Circularity
NS.
*
Female
Male
E
F
G
Wall area percent [WA%]
TB cross-sectional area [mm^2]
Alveolar Attachment Adj.
***

Fig. 6

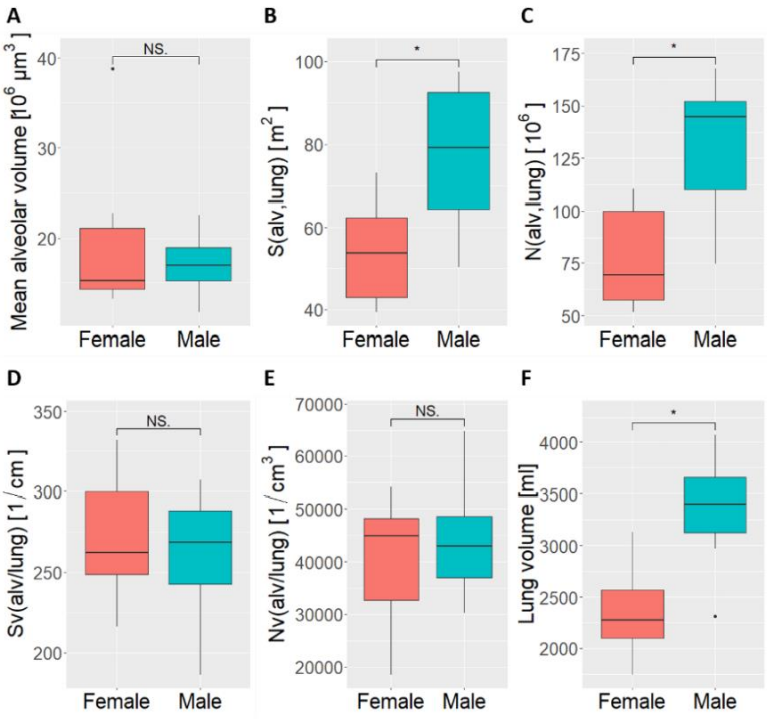
A
Mean alveolar volume [10^6 µm^3]
NS.
Female
Male
B
S(alv,lung) [m^2]
*
C
N(alv,lung) [10^6]
D
Sv(alv/lung) [1/cm]
E
Nv(alv/lung) [1/cm^3]
F
Lung volume [ml]

Fig. 7

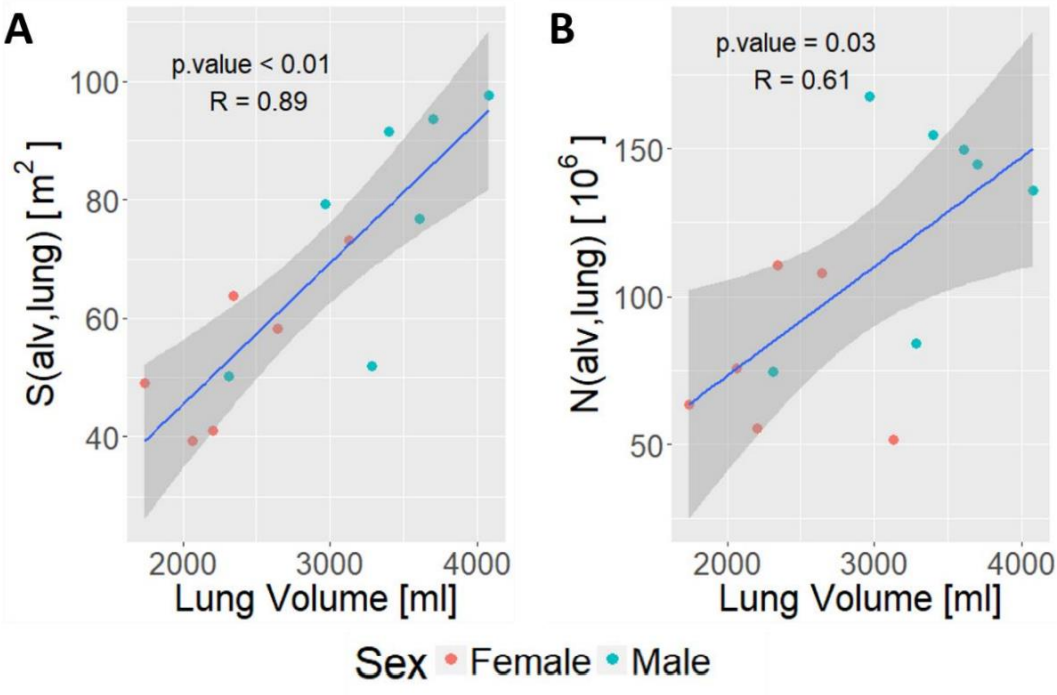
A
p.value < 0.01
R = 0.89
S(alv,lung) [m^2]
Lung Volume [ml]
B
p.value = 0.03
R = 0.61
N(alv,lung) [10^6]
Lung Volume [ml]
Sex Female Male

Fig. 8

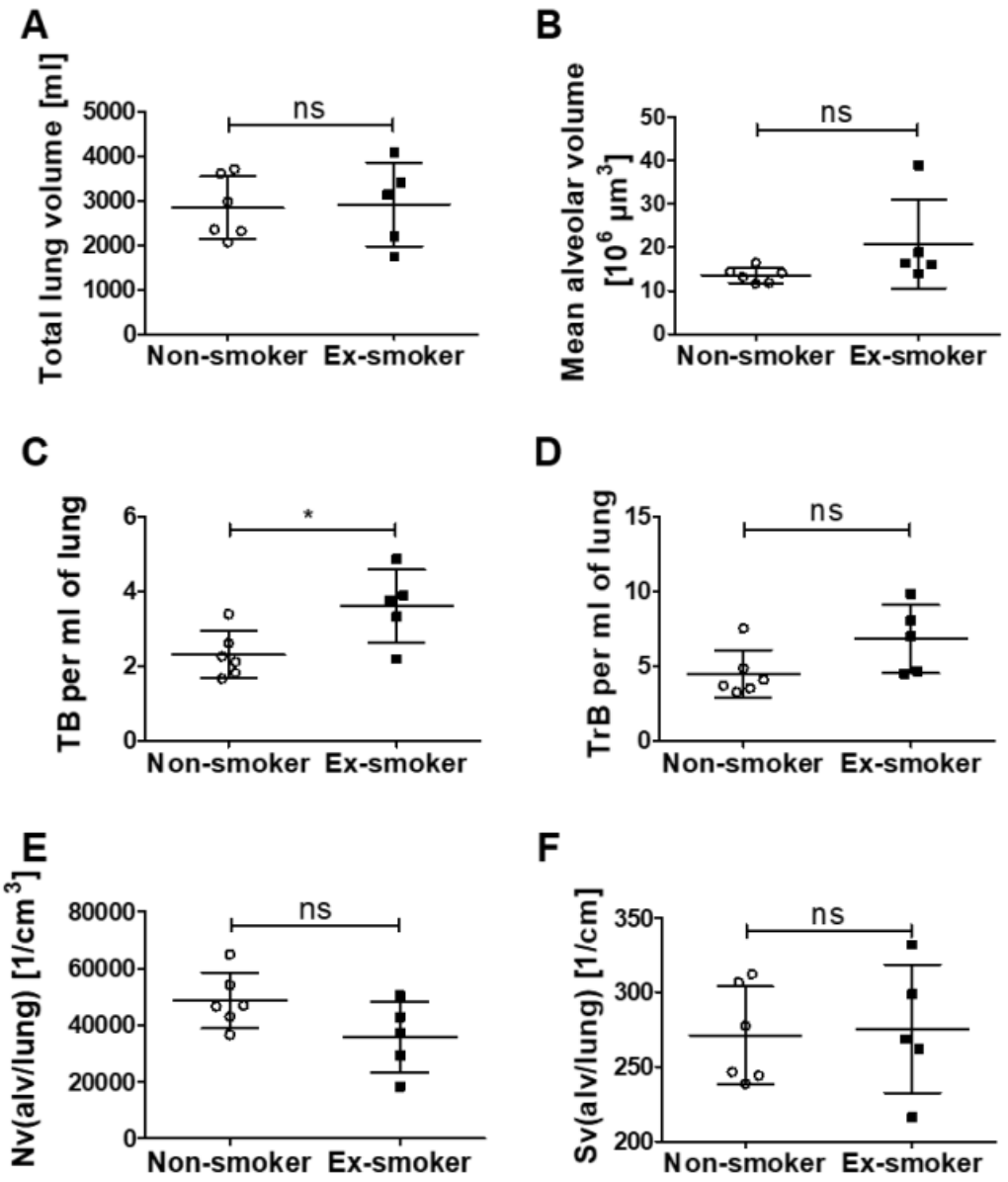
A
Total lung volume [ml]
5000
4000
3000
2000
1000
0
ns
Non-smoker
Ex-smoker
B
Mean alveolar volume [10^6 µm^3]
50
40
30
20
10
0
ns
Non-smoker
Ex-smoker
C
TB per ml of lung
6
4
2
0
*
Non-smoker
Ex-smoker
D
TrB per ml of lung
15
10
5
0
ns
Non-smoker
Ex-smoker
E
Nv(alv/lung) [1/cm^3]
80000
60000
40000
20000
0
ns
Non-smoker
Ex-smoker
F
Sv(alv/lung) [1/cm]
350
300
250
200
ns
Non-smoker
Ex-smoker

VIII. Figure Captions

Figure 1: Stereological sampling of air inflated frozen lungs

A. Representative image of an air inflated frozen right lung specimen used in this study. Yellow lines indicate how the lung was sliced into 2cm thick slices using a pre-cooled band saw. B. The whole lung is scanned using computed tomography (CT) prior to slicing to enable segmentation and calculation of the total lung volume. The white dashed box indicates the location of CT slice visualized in figure 1C. C. The orientation of the CT scan is matched to the lung slice photographs. A point grid is applied to the CT images to determine the parenchymal volume fraction. D. Example photo of the lung slice matching figure 1C with a randomly placed digital grid used to determine systematic uniform random (SUR) samples. Red arrows indicate sampling sites that were excluded from sampling because they fell on a fissure gap or non-parenchymal features such as large airways or blood vessels.

Figure 2: Intersection analysis of whole lung and SUR sample histograms

A. 3D rendering of the systematic uniform random (SUR) sample locations are displayed together with the sagittal and transaxial images of the CT scan to visualize the uniform distribution of the samples taken. The CT data at the registered locations of the SUR samples was used to calculate the histogram similarity between the voxel based density distribution of the whole lung and the SUR sample locations. The density distribution of the whole lung and SUR samples was compared to demonstrate the level of representativeness of the samples. B. The best match between whole lung histogram and histogram of SUR sample locations. C. Median case of histogram matchings. D. Worst histogram match.

Figure 3: Stereological counting probes applied to microCT images of human lung tissue samples

A. Example microCT image with randomly overlaid checkered line grid (line length 1mm). Line intercepts with alveolar tissue were counted (pink stars; each star indicates one crossing of the line from air space into tissue or from tissue into air space). End of lines were used to count parenchymal features (alveoli (yellow), alveolar ducts (green), septal walls (turquoise) and non-parenchyma (red)). The sub-panel shows a magnified view of the area with just one of the line to better illustrate the ability to distinguish line intercepts (white arrow heads). B. An image pair (disector) used to count appearance of an alveolar wall called a "bridge". For that, images were loaded into the STEPanizer program which projected a counting frame (red) on all images. Solid part of frame line indicates the forbidden line and alveoli touching or intersecting with it are not counted, while alveoli intersecting or touching the dotted line are included. C. An oblique view through a microCT scan was generated to show a longitudinal cut through a terminal bronchiole and its daughter branches (transitional bronchioles, the first order respiratory bronchioles). The image was paired with a schematic of the sibling airway branching structure and provides the means to highlight the method used to unambiguously label the airways at the transition from the conducting to the respiratory zone (i.e. terminal and transitional bronchioles).

Figure 4: 3D visualization of conducting and respiratory bronchioles imaged by microCT

A. 3D rendering of segmented airway tree with orthogonal microCT images (sagittal and transaxial) of a tissue sample. Conducting airways are colored in orange, while respiratory bronchioles are colored in light blue. B. Skeleton overlaid onto the 3D rendering of the airway tree. Branch-points are indicated as spheres in magenta, endpoints of branches in blue and points at which cross-sectional images were computed in red. Eleven cross-sectional images along a terminal bronchiole are computed at 10% intervals starting from the center of the branch and moving towards the end points. C. Three example cross-sectional images through one of the

TB's are shown (red arrows in B). Automatically detected airway walls are outlined with a yellow line. A blood vessel drained of blood is shown next to the airway.

Figure 5: Comparison of terminal bronchioles in males and females

A. The number of terminal (TB) and B. transitional bronchioles per lung between males (n=7) and females (n=6). The morphometry terminal bronchioles from males n=68 and females n=54 was assessed for: C. length, D. circularity, E. wall area percent, F. cross-sectional area and G. number of alveolar attachments adjusted for perimeter length. *: $p<0.05$; ***: $p<0.001$; NS. (not significant): $p>0.05$.

Figure 6: Comparison of parenchymal morphometry in males and females

A. The number weighted mean alveolar volume, B. total alveolar surface (S(alv,lung)), C. total number of alveoli (N(alv,lung)), D. alveolar surface density (Sv(alv/lung)), E. alveolar number density (Nv(alv/lung)) and F. the total lung volume were compared between males (n=7) and females (n=6). *: $p<0.05$; NS. (not significant): $p>0.05$.

Figure 7: Correlations of total alveolar surface area and number of alveoli with Lung Volume

Correlations of A. The total alveolar surface area (S(alv,lung)) and B. The total number of alveoli per lung (N(alv,lung)) with lung volume. Spearman rank correlation was used to calculate the p value and rho value.

Figure 8: Comparison with smoking status

Data per lung was divided into subjects that did not have any smoking history (n=6) and subjects with a history of smoking (n=5). Comparison between smokers and never-smokers was

performed for A. total lung volume, B. mean alveolar volume, C. number of terminal bronchioles (TB) and D. transitional bronchioles (TrB) per ml of lung, E. alveolar density (Nv(alv/lung)) and F. surface density (Sv(alv/lung). Simple t-test was used to calculate significance. *: $p<0.05$

IX. References

1. **Camp PG**, **Coxson HO**, **Levy RD**, **Pillai SG**, **Anderson W**, **Vestbo J**, **Kennedy SM**, **Silverman EK**, **Lomas DA**, **Pare PD**. Sex differences in emphysema and airway disease in smokers. *Chest* 136: 1480–1488, 2009.

2. **Coxson HO**, **Mayo JR**, **Behzad H**, **Moore BJ**, **Verburgt LM**, **Staples CA**, **Pare PD**, **Hogg JC**. Measurement of lung expansion with computed tomography and comparison with quantitative histology. *J Appl Physiol* 79: 1525–1530, 1995.

3. **Diaz AA**, **Estepar RS**, **Washko GR**. Computed Tomographic Airway Morphology in Chronic Obstructive Pulmonary Disease. Remodeling or Innate Anatomy? *Ann Am Thorac Soc* 13: 4–9, 2016.

4. **Dominelli PB**, **Ripoll JG**, **Cross TJ**, **Baker SE**, **Wiggins CC**, **Welch BT**, **Joyner MJ**. Sex differences in large conducting airway anatomy. *J Appl Physiol* 125: 960–965, 2018.

5. **Dunnill MS**. Postnatal Growth of the Lung [Online]. *Thorax* 17: 329–333, 1962. https://www.ncbi.nlm.nih.gov/pmc/articles/PMC1018719/.

6. **Gehr P**, **Bachofen M**, **Weibel ER**. The normal human lung: ultrastructure and morphometric estimation of diffusion capacity [Online]. *Respir Physiol* 32: 121–140, 1978. http://www.ncbi.nlm.nih.gov/pubmed/644146.

7. **Grydeland TB**, **Dirksen A**, **Coxson HO**, **Pillai SG**, **Sharma S**, **Eide GE**, **Gulsvik A**, **Bakke PS**. Quantitative computed tomography: emphysema and airway wall thickness by sex, age and smoking. *Eur Respir J* 34: 858–865, 2009.

8. **Gundersen HJ**, **Jensen EB**, **Kieu K**, **Nielsen J**. The efficiency of systematic sampling in stereology--reconsidered [Online]. *J Microsc* 193: 199–211, 1999. http://www.ncbi.nlm.nih.gov/pubmed/10348656.

9. **Haefeli-Bleuer B**, **Weibel ER**. Morphometry of the human pulmonary acinus. *Anat Rec* 220: 401–414, 1988.

10. **Herring MJ**, **Putney LF**, **Wyatt G**, **Finkbeiner WE**, **Hyde DM**. Growth of alveoli during postnatal development in humans based on stereological estimation. *Am J Physiol Lung Cell Mol Physiol* 307: L338-44, 2014.

11. **Hislop AA**, **Wigglesworth JS**, **Desai R**. Alveolar development in the human fetus and infant [Online]. *Early Hum Dev* 13: 1–11, 1986. http://www.ncbi.nlm.nih.gov/pubmed/3956418.

12. **Hoffman EA**, **Ahmed FS**, **Baumhauer H**, **Budoff M**, **Carr JJ**, **Kronmal R**, **Reddy S**, **Barr RG**. Variation in the percent of emphysema-like lung in a healthy, nonsmoking multiethnic sample. The MESA lung study. *Ann Am Thorac Soc* 11: 898–907, 2014.

13. **Hoffman EA**, **Olsen LE**. Characteristics of Respiratory System Complexity Captured via X-Ray Computed Tomography: Image Acquisition, Display, and Analysis [Online]. Taylor & Francis. https://library.villanova.edu/Find/Record/514493/TOC.

14. **Hoffman EA**, **Sinak LJ**, **Robb RA**, **Ritman EL**. Noninvasive quantitative imaging of shape and volume of lungs. *J Appl Physiol Respir Env Exerc Physiol* 54: 1414–1421, 1983.

15. **Hsia CC**, **Hyde DM**, **Ochs M**, **Weibel ER**, **Structure AEJTF on QA of L**. An official research policy statement of the American Thoracic Society/European Respiratory Society: standards for quantitative assessment of lung structure. *Am J Respir Crit Care Med* 181: 394–418, 2010.

16. **Hyde DM**, **Tyler NK**, **Plopper CG**. Morphometry of the respiratory tract: avoiding the sampling, size, orientation, and reference traps. *Toxicol Pathol* 35: 41–48, 2007.

17. **Hyde DM**, **Tyler NK**, **Putney LF**, **Singh P**, **Gundersen HJ**. Total number and mean size of alveoli in mammalian lung estimated using fractionator sampling and unbiased estimates of the Euler characteristic of alveolar openings. *Anat Rec A Discov Mol Cell Evol Biol* 277: 216–226, 2004.

18. **Johns RA**, **Steude JS**, **Castanier LM**, **Roberts P V**. Nondestructive measurements of fracture aperture in crystalline rock cores using X ray computed tomography. *J Geophys Res Solid Earth* 98: 1889–1900, 1993.

19. **Kim YI**, **Schroeder J**, **Lynch D**, **Newell J**, **Make B**, **Friedlander A**, **Estepar RS**, **Hanania NA**, **Washko G**, **Murphy JR**, **Wilson C**, **Hokanson JE**, **Zach J**, **Butterfield K**, **Bowler RP**, **Copdgene I**. Gender differences of airway dimensions in anatomically matched sites on CT in smokers. *COPD* 8: 285–292, 2011.

20. **Knudsen L**, **Weibel ER**, **Gundersen HJ**, **Weinstein F V**, **Ochs M**. Assessment of air space size characteristics by intercept (chord) measurement: an accurate and efficient stereological approach. *J Appl Physiol* 108: 412–421, 2010.

21. **Knust J**, **Ochs M**, **Gundersen HJ**, **Nyengaard JR**. Stereological estimates of alveolar number and size and capillary length and surface area in mice lungs. *Anat Rec* 292: 113–122, 2009.

22. **Koo HK**, **Vasilescu DM**, **Booth S**, **Hsieh A**, **Katsamenis OL**, **Fishbane N**, **Elliott WM**, **Kirby M**, **Lackie P**, **Sinclair I**, **Warner JA**, **Cooper JD**, **Coxson HO**, **Paré PD**, **Hogg JC**, **Hackett TL**. Small airways disease in mild and moderate chronic obstructive pulmonary disease: a cross-sectional study. *Lancet Respir Med* 6: 591–602, 2018.

23. **Kurashima K**, **Hoshi T**, **Takaku Y**, **Kanauchi T**, **Nakamoto K**, **Ueda M**, **Takayanagi N**, **Colby T V**, **Sugita Y**, **Kawabata Y**. Changes in the airway lumen and surrounding parenchyma in chronic obstructive pulmonary disease. *Int J Chron Obs Pulmon Dis* 8: 523–532, 2013.

24. **Langston C**, **Waszkiewicz E**, **Thurlbeck WM**. A simple method for the representative sampling of lungs of diverse size [Online]. *Thorax* 34: 527–530, 1979. http://www.ncbi.nlm.nih.gov/pubmed/505350.

25. **Litzlbauer HD**, **Korbel K**, **Kline TL**, **Jorgensen SM**, **Eaker DR**, **Bohle RM**, **Ritman EL**, **Langheinrich AC**. Synchrotron-based micro-CT imaging of the human lung acinus.

Anat Rec 293: 1607–1614, 2010.

26. **Lynch DA**, **Austin JH**, **Hogg JC**, **Grenier PA**, **Kauczor HU**, **Bankier AA**, **Barr RG**, **Colby T V**, **Galvin JR**, **Gevenois PA**, **Coxson HO**, **Hoffman EA**, **Newell Jr. JD**, **Pistolesi M**, **Silverman EK**, **Crapo JD**. CT-Definable Subtypes of Chronic Obstructive Pulmonary Disease: A Statement of the Fleischner Society. *Radiology* 277: 192–205, 2015.

27. **Martinez FJ**, **Curtis JL**, **Sciurba F**, **Mumford J**, **Giardino ND**, **Weinmann G**, **Kazerooni E**, **Murray S**, **Criner GJ**, **Sin DD**, **Hogg J**, **Ries AL**, **Han M**, **Fishman AP**, **Make B**, **Hoffman EA**, **Mohsenifar Z**, **Wise R**, **National Emphysema Treatment Trial Research G**. Sex differences in severe pulmonary emphysema. *Am J Respir Crit Care Med* 176: 243–252, 2007.

28. **McDonough JE**, **Knudsen L**, **Wright AC**, **Elliott W**, **Ochs M**, **Hogg JC**. Regional differences in alveolar density in the human lung are related to lung height. *J Appl Physiol* 118: 1429–1434, 2015.

29. **McDonough JE**, **Yuan R**, **Suzuki M**, **Seyednejad N**, **Elliott WM**, **Sanchez PG**, **Wright AC**, **Gefter WB**, **Litzky L**, **Coxson HO**, **Pare PD**, **Sin DD**, **Pierce RA**, **Woods JC**, **McWilliams AM**, **Mayo JR**, **Lam SC**, **Cooper JD**, **Hogg JC**. Small-airway obstruction and emphysema in chronic obstructive pulmonary disease. *N Engl J Med* 365: 1567–1575, 2011.

30. **Mühlfeld C**, **Knudsen L**, **Ochs M**. Stereology and Morphometry of Lung Tissue. 2012, p. 367–390.

31. **Muhlfeld C**, **Ochs M**. Quantitative microscopy of the lung: a problem-based approach. Part 2: stereological parameters and study designs in various diseases of the respiratory tract. *Am J Physiol Lung Cell Mol Physiol* 305: L205-21, 2013.

32. **Muller NL**, **Staples CA**, **Miller RR**, **Abboud RT**. "Density mask". An objective method to quantitate emphysema using computed tomography [Online]. *Chest* 94: 782–787, 1988. http://www.ncbi.nlm.nih.gov/pubmed/3168574.

33. **Ochs M**, **Nyengaard JR**, **Jung A**, **Knudsen L**, **Voigt M**, **Wahlers T**, **Richter J**, **Gundersen HJ**. The number of alveoli in the human lung. *Am J Respir Crit Care Med* 169: 120–124, 2004.

34. **Park JO**, **Choi IS**, **Park KO**. Normal predicted values of single-breath diffusing capacity of the lung in healthy nonsmoking adults. *Korean J Intern Med* 1: 178–184, 1986.

35. **Patel BD**, **Coxson HO**, **Pillai SG**, **Agusti AG**, **Calverley PM**, **Donner CF**, **Make BJ**, **Muller NL**, **Rennard SI**, **Vestbo J**, **Wouters EF**, **Hiorns MP**, **Nakano Y**, **Camp PG**, **Nasute Fauerbach P V**, **Screaton NJ**, **Campbell EJ**, **Anderson WH**, **Pare PD**, **Levy RD**, **Lake SL**, **Silverman EK**, **Lomas DA**, **International CGN**. Airway wall thickening and emphysema show independent familial aggregation in chronic obstructive pulmonary disease. *Am J Respir Crit Care Med* 178: 500–505, 2008.

36. **Peyton RL**, **Haeffner BA**, **Anderson SH**, **Gantzer CJ**. Applying X-ray CT to measure

macropore diameters in undisturbed soil cores. *Geoderma* 53: 329–340, 1992.

37. **Pump KK**. Morphology of the acinus of the human lung [Online]. *Dis Chest* 56: 126–134, 1969. http://www.ncbi.nlm.nih.gov/pubmed/5798864.

38. **Rodriguez M**, **Bur S**, **Favre A**, **Weibel ER**. Pulmonary acinus: geometry and morphometry of the peripheral airway system in rat and rabbit. *Am J Anat* 180: 143–155, 1987.

39. **Tan WC**, **Hague CJ**, **Leipsic J**, **Bourbeau J**, **Zheng L**, **Li PZ**, **Sin DD**, **Coxson HO**, **Kirby M**, **Hogg JC**, **Raju R**, **Road J**, **O'Donnell DE**, **Maltais F**, **Hernandez P**, **Cowie R**, **Chapman KR**, **Marciniuk DD**, **FitzGerald JM**, **Aaron SD**, **Canadian Respiratory Research N**, **the Can CCR group**. Findings on Thoracic Computed Tomography Scans and Respiratory Outcomes in Persons with and without Chronic Obstructive Pulmonary Disease: A Population-Based Cohort Study. *PLoS One* 11: e0166745, 2016.

40. **Tanabe N**, **Vasilescu DM**, **Kirby M**, **Coxson HO**, **Verleden SE**, **Vanaudenaerde BM**, **Kinose D**, **Nakano Y**, **Pare PD**, **Hogg JC**. Analysis of airway pathology in COPD using a combination of computed tomography, micro-computed tomography and histology. *Eur Respir J* 51, 2018.

41. **Tanabe N**, **Vasilescu DM**, **McDonough JE**, **Kinose D**, **Suzuki M**, **Cooper JD**, **Pare PD**, **Hogg JC**. Micro-Computed Tomography Comparison of Preterminal Bronchioles in Centrilobular and Panlobular Emphysema. *Am J Respir Crit Care Med* 195: 630–638, 2017.

42. **Thurlbeck WM**. The internal surface area of nonemphysematous lungs. *Am Rev Respir Dis* 95: 765–773, 1967.

43. **Tschanz SA**, **Burri PH**, **Weibel ER**. A simple tool for stereological assessment of digital images: the STEPanizer. *J Microsc* 243: 47–59, 2011.

44. **Turgeon ML**. Clinical Hematology: Theory and Procedures [Online]. Lippincott Williams & Wilkins. https://books.google.ca/books?id=cHAjsUgegpQC.

45. **Vasilescu DM**, **Gao Z**, **Saha PK**, **Yin L**, **Wang G**, **Haefeli-Bleuer B**, **Ochs M**, **Weibel ER**, **Hoffman EA**. Assessment of morphometry of pulmonary acini in mouse lungs by nondestructive imaging using multiscale microcomputed tomography. *Proc Natl Acad Sci U S A* 109: 17105–17110, 2012.

46. **Vasilescu DM**, **Klinge C**, **Knudsen L**, **Yin L**, **Wang G**, **Weibel ER**, **Ochs M**, **Hoffman EA**. Stereological assessment of mouse lung parenchyma via nondestructive, multiscale micro-CT imaging validated by light microscopic histology. *J Appl Physiol* 114: 716–724, 2013.

47. **Vasilescu DM**, **Phillion AB**, **Tanabe N**, **Kinose D**, **Paige DF**, **Kantrowitz JJ**, **Liu G**, **Liu H**, **Fishbane N**, **Verleden SE**, **Vanaudenaerde BM**, **Lenburg M**, **Stevenson CS**, **Spira A**, **Cooper JD**, **Hackett TL**, **Hogg JC**. Nondestructive cryomicro-CT imaging enables structural and molecular analysis of human lung tissue. *J Appl Physiol* 122: 161–169, 2017.

48. **Verleden SE**, **Vasilescu DM**, **Willems S**, **Ruttens D**, **Vos R**, **Vandermeulen E**, **Hostens J**, **McDonough JE**, **Verbeken EK**, **Verschakelen J**, **Van Raemdonck DE**, **Rondelet B**, **Knoop C**, **Decramer M**, **Cooper J**, **Hogg JC**, **Verleden GM**, **Vanaudenaerde BM**. The site and nature of airway obstruction after lung transplantation. *Am J Respir Crit Care Med* 189: 292–300, 2014.

49. **Washko GR**, **Parraga G**, **Coxson HO**. Quantitative pulmonary imaging using computed tomography and magnetic resonance imaging. *Respirology* 17: 432–444, 2012.

50. **Watz H**, **Breithecker A**, **Rau WS**, **Kriete A**. Micro-CT of the human lung: imaging of alveoli and virtual endoscopy of an alveolar duct in a normal lung and in a lung with centrilobular emphysema--initial observations. *Radiology* 236: 1053–1058, 2005.

51. **Weibel ER**. Morphometry of the human lung [Online]. Academic Press. https://books.google.ca/books?id=ebhqAAAAMAAJ.

52. **Weibel ER**. Stereological Methods: Practical methods for biological morphometry [Online]. Academic Press. https://books.google.ca/books?id=_SJBAAAAYAAJ.

53. **Weibel ER**, **Gomez DM**. Architecture of the human lung. Use of quantitative methods establishes fundamental relations between size and number of lung structures [Online]. *Science (80-)* 137: 577–585, 1962. http://www.ncbi.nlm.nih.gov/pubmed/14005590.

54. **Wellington SL**, **Vinegar HJ**. X-ray computerized tomography [Online]. *J Pet Technol* 39: 885–898, 1987. http://inis.iaea.org/search/search.aspx?orig_q=RN:19005948.

55. **West JB**. Respiratory Physiology: People and Ideas; Chapter 1: The Structural Basis of Lung Function by Ewald R. Weibel [Online]. Springer New York. https://books.google.ca/books?id=KnXgBwAAQBAJ.

56. **Wiebe BM**, **Laursen H**. Human lung volume, alveolar surface area, and capillary length. *Microsc Res Tech* 32: 255–262, 1995.

57. **Wiebe BM**, **Laursen H**. Lung morphometry by unbiased methods in emphysema: bronchial and blood vessel volume, alveolar surface area and capillary length [Online]. *APMIS* 106: 651–656, 1998. http://www.ncbi.nlm.nih.gov/pubmed/9725798.

58. **Wood SA**, **Zerhouni EA**, **Hoford JD**, **Hoffman EA**, **Mitzner W**. Measurement of three-dimensional lung tree structures by using computed tomography. *J Appl Physiol* 79: 1687–1697, 1995.

59. **Zach JA**, **Newell Jr. JD**, **Schroeder J**, **Murphy JR**, **Curran-Everett D**, **Hoffman EA**, **Westgate PM**, **Han MK**, **Silverman EK**, **Crapo JD**, **Lynch DA**, **Investigators COpdg**. Quantitative computed tomography of the lungs and airways in healthy nonsmoking adults. *Invest Radiol* 47: 596–602, 2012.